Development and Performance of a Digital Image Radiometer for Heliostat Evaluation at Solar One

J. B. Blackmon
McDonnell Douglas Astronautics Co.,
Huntington Beach, Calif. 92647

A review is presented of the development, performance, and operation of a digital image radiometer (DIR) used to evaluate and enhance heliostat optical and tracking performance at the Solar One 10 MWe pilot plant at Daggett, Calif. The system, termed the beam characterization system (BCS), is based on digitizing, calibrating, and computer-processing video images of heliostat-reflected beams displayed on four 30- by 40-ft targets located on the tower beneath the receiver. Additionally, the radiance distribution of the sun is simultaneously recorded by a separate, specially modified solar-tracking video camera. The basic theory and analytical techniques used to determine beam centroid error (i.e., heliostat pointing errors), the actual incident beam power, spillage power off the receiver, and solar radiance distribution are described. The computer system is presented including the automatic data acquisition mode, the interface with the heliostat array controller (HAC), and the data acquisition system (DAS). Data display for plant operator purposes and additional data acquired and stored for more detailed engineering evaluations are discussed. Advanced applications of the DIR such as determination of total incident flux on a receiver from a field of heliostats, reflectance monitoring, and measurement of atmospheric attenuation are presented.

Introduction

Early in the development of solar central receivers, it was recognized that some means of aligning, monitoring, and evaluating large numbers of heliostats would be required. To meet these objectives, a digital image radiometer (DIR) was conceived in 1974 at McDonnell Douglas Astronautics Co. as part of a company-funded solar research and development program. This early DIR system consisted of a video camera, video digitizer, elevated target with several radiometers, and computers. This system was used to evaluate heliostats in desert tests conducted in 1974–1975 and 1976–1977 at the Naval Weapons Center [1]. Results showed that total beam power, irradiance distribution, beam centroid, tracking accuracy, and overall mirror reflectance were accurately and rapidly determinable. This early system was also used to determine the sun's radiance distribution.

An improved version was installed in late 1977 at the MDAC Huntington Beach Solar Energy Test Facility and used to evaluate various mirror modules and heliostats. A similar device was developed at Sandia National Laboratories Central Receiver Test Facility in 1979, and used extensively in the evaluation of various heliostats [2–6].

The basic DIR approach was originally selected because it offered high resolution, high acquisition rates, and real-time visual monitoring, used passive targets, required little maintenance, and was the lowest cost system when compared with calorimeters or arrays of moving or stationary point detectors mounted on the tower.

These advantages, coupled with successful experience with the first DIR systems at MDAC and Sandia, led to selection of the DIR as the beam characterization system (BCS) at the Solar One 10 MWe pilot plant in Daggett, Calif. Additional requirements imposed on this system involved automatic operation, sophisticated integration with other subsystems, and a variety of options for acquiring, storing, and analyzing on-line and off-line data. This system provides an automatic update of heliostat-tracking-aimpoint biases and monitors heliostat optical performance; it has been operational since September 1982 [7]. Improvements were made in 1984, such as the addition of a camera to track the sun and determine the solar radiance distribution simultaneously with each beam scan. The BCS now provides comparisons of observed beam shape with computer codes that use solar radiance distribution data and theoretical heliostat optical characteristics to evaluate performance.

Beam Characterization System (BCS) Design

The Solar One beam characterization system characterizes the reflected beam from a heliostat or mirror module, with respect to flux distribution and beam size, shape, centroid, and power. The BCS is used to align and evaluate heliostats as part of the pilot plant functional and integrated acceptance test program, and provides operational support for collector subsystem realignment, performance evaluation, and maintenance throughout plant operation. The overall system

Contributed by the Solar Energy Division and presented at the Solar Energy Conference, Las Vegas, Nev., 1984. Manuscript received by the Solar Energy Division, November, 1984.

design and special component design features are described below.

System Design. The BCS is based on the DIR measuring and recording instrument and is shown in Figs. 1 and 2. The basic BCS consists of four video cameras, each of which views an elevated target mounted on the tower beneath the receiver. The video analog output signals are digitized to provide a mesure of beam intensity incident on each target from a heliostat. The digitized intensity for a particular frame is correlated with absolute intensity measurements made nearly simultaneously by a calibration procedure that uses three target-mounted radiometers. The targets are flat metal structures painted with a high-temperature white paint having near-Lambertian reflectance characteristcs to minimize glare and provide uniform reflectance over the target surface.

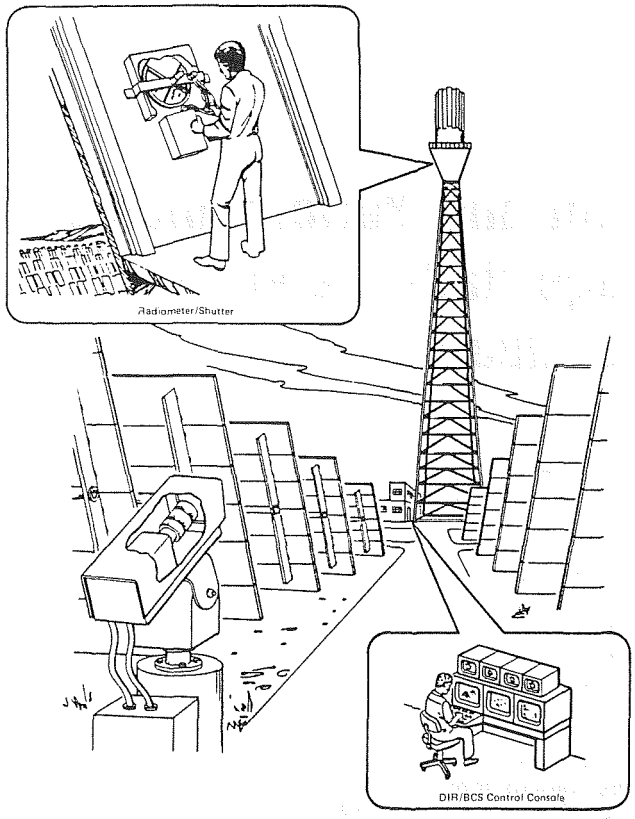

Fig. 1 Digital image radiometer beam characterization subsystem

Simultaneous measurements of the sun's radiance distribution are made with a specially modified video camera that tracks the sun. These data, coupled with the absolute measurements of incident irradiance, are used in computer codes that compare actual and theoretically ideal heliostat irradiance distributions.

Additional radiometers located in the field as part of the data acquisition subsystem (DAS) determine incident solar irradiance, which is used to establish heliostat reflective efficiency as measured at the target. Beam centroid data are obtained to establish heliostat aimpoints.

Component Design Features

Video Camera. The video camera is a Model 2850C-207 low-light television camera manufactured by COHU, Inc., Electronics Division. The camera is equipped with an RCA Model 4532 B/H silicon diode array vidicon tube and a COHU Model 2820 C-204 10:1 zoom lens with a 2X extender. Features include remote or automatic iris and zoom control, antiglare shields, sealed environmental housing, dual-tone modulated frequency (DTMF) control from the BCS computer interface, and a stable platform to minimize camera movement and wind-induced vibration.

The antiglare shields eliminate stray light from clouds,

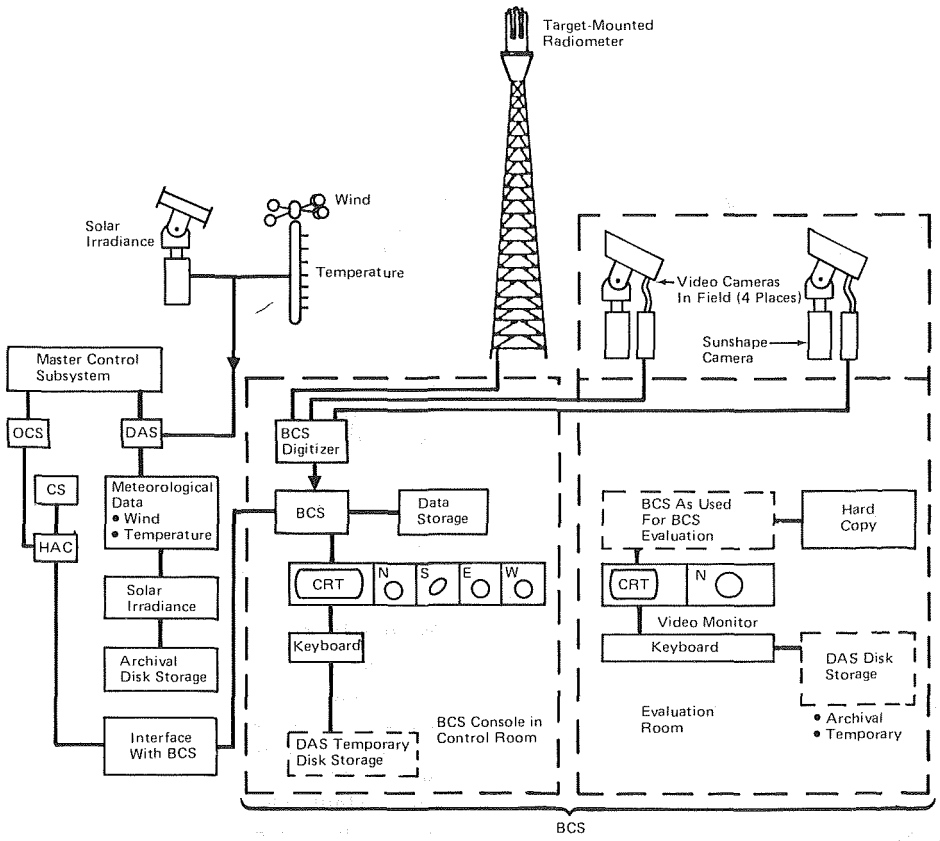

Fig. 2 BCS interface block flow diagram

receiver, sun, etc., which could cause erroneous measurements. The shields are formed to match the shape of the target and two or three are used as multiple light baffles.

Circuit modifications eliminate automatic gain control types of responses and a black-level mask located at the edge of the image is used as a reference to ensure constant black level over a wide temperature range. These modifications allow the camera to operate as a radiometer, with light level controlled by iris settings and filters.

The camera has a relay lens for the black-level mask and space for a variety of filters used to flatten the response of the camera over its spectral response range.

Dual Tone Modulated Frequency (DTMF) Camera Control System. Camera selection and light control are accomplished by a noise-resistant tone-command system composed of a transmitter in the camera control rack and a remote receiver near each camera.

The transmitter is a COHU Model DTMF 100 modified for Solar One application. Integral manual control switches are provided to select the desired camera, apply power, and control the iris or place it in automatic mode. Reed relay outputs from the MODCOMP Model 1136 module in the BCS computer provide programmable camera selection and iris control. Camera control commands are encoded to digital form and transmitted to the selected receiver over standard twisted-pair wires using audio tones to represent the digital information. The transmitter also sends camera-select commands to route the desired video input through the video switch to the digitizer.

The COHU Model DTMF 200 receiver decodes the command data from the transmitter and provides power and iris control commands to the associated video camera.

Video Switch. The video switch is a Pelco Model VS504R switching matrix, which routes the selected video input (north, south, east, west, or sunshape camera) to the video digitizer.

Video Digitizer. The video digitizer system is a Quantex Model DS-12 digital image memory/processor. This system (1) accepts the video signal from the video camera (conforming to the EIA RS-170 standard), (2) converts the signal to a digital form, (3) stores the digital data, and (4) transmits the data to the BCS computer upon command over an IEEE 488 interface.

Incoming composite video is stripped of sync and applied to a high-speed A/D converter. Data from the A/D passes through the arithmetic process where it may be combined with a memory data through hardwired arithmetic processes that include summation with data already in memory, averaging, and subtraction. The resulting data are then stored in memory.

The IEEE 488 interface connects the digital memory port and the system control microprocessor to the MODCOMP Model 5488 controller in the BCS computer. This interface connects the digitizer to a direct memory access channel of the BCS computer and allows block transfer of image data and program control of the digitizer functions.

A standard EIA RS-170 video output is routed to the BCS monitor CRT in the receiver console in the control room. Processed data are routed through a D/A converter to the digitizer or unprocessed data may be selected.

Operation. Automatic BCS operation normally occurs when the plant is operational. Heliostats are automatically selected from a file, or heliostat candidate list, so that 60 heliostats can be tested each day. To avoid stray beams from heliostats in an adjacent quadrant, opposite quadrants and targets are tested; that is, the north and south field heliostat beams are sequentially moved onto the north and south targets while the east and west field heliostats continue to track on the receiver. Later, the east and west field heliostats are sequentially tested.

Three runs are taken during the day (morning, noon, afternoon) so that the tracking aimpoint variations can be assessed and a nominal aimpoint selected. This procedure is used because heliostat aimpoints often exhibit a diurnal variation.

At the end of the day, the aimpoint data, based on the measured beam intensity centroids, are used to bias the heliostat tracking data in the heliostat array controller (HAC) and thus correct the aimpoint.

The HAC controls the heliostats so that each beam is moved on and off the target as required. As each selected heliostat is trained on the target, the appropriate video camera is switched to view the beam and the video signal is digitized and transmitted to the BCS computer. The BCS computer processes the digitized data, correlates the data with absolute intensity measured by target-mounted radiometers, and outputs the processed data on a CRT display terminal that has hardcopy capability.

A computer program resident in the BCS determines which heliostats could block or shadow the test heliostat. The beam from the test heliostat is then moved from the receiver to a standby aimpoint, the interfering heliostats are commanded to face-up stow positions, and the test heliostat beam is then directed at the target. The 8-bit video digitizer takes an "image grab" and the computer analyzes the data. If the beam is too bright (the digitizer shows saturated values) or too dim (peak values less then 150), the camera iris is adjusted automatically to obtain the correct brightness range. Five image grabs are then taken and stored in rapid succession.

A calibration curve is constructed from the digitized brightness values at the three points on the target where the radiometers are located and the corresponding radiometer measurements of irradiance (W/m^2). A total of 15 data points is obtained, from which a curve relating brightness to irradiance is determined. A message is then sent from the BCS to the HAC that the beam scans are complete, the HAC moves the beam off the target, and a rapid series of background image grabs is taken. The background brightness values are subtracted from the previous beam brightness values taken 5 to 30 seconds previously. The calibration curve is used to obtain the net irradiance corresponding to each pizel. Calculations are then made of beam centroid, beam power, spillage power, etc., as described in the following sections.

Immediately after the last beam scan, an image grab is taken of the sun and the corresponding irradiance is measured by an adjacent Eppley pyrheliometer. Correlation of the digitized video image of the sun and the measured irradiance gives the radiance (W/m^2 steradian).

This procedure is followed sequentially at a rate of roughly 15 to 30 heliostats per hour with most of this time period required for repositioning interfering heliostats.

Principle of Operation. The BCS acquires a large number (256×256) of relative brightness values (termed DIR numbers) with a video scan. These qualitative brightness data can be transformed into quantitative irradiance data using the calibration technique that associates the brightness at several points on the target with simultaneous, quantitative radiometer measurements taken at those points. The calibration curve obtained is then applied to all of the brightness values so that the irradiance at each pixel, the net beam power, the centroid of the beam, and the isoflux contours can be determined.

In order to achieve reasonable accuracies, however, a number of requirements must be met, as discussed below.

Alignment. The principal requirement for accurate power measurement is that the beam must cover at least one of the three central radiometers, preferably with the higher irradiance region of the beam. Because the Solar One heliostats

have a single mirror-module cant angle configuration, beam irradiance for outer row heliostats shows a central maximum and a gradual decrease with increasing radius from the beam center. Close-in heliostats show little overlap and exhibit a great deal of nonuniformity; each mirror module is distinguishable, as are the spaces between the modules. As a result, close-in heliostats may cover a radiometer with a rapidly varying irradiance distribution or slope, and heliostat movement further changes the irradiance on the radiometer. These effects decrease accuracy by increasing the data spread for the calibration curve. Power measurement accuracy is therefore greater for outer field heliostats that normally give good calibration-curve results. Because of this close-in heliostat nonuniformity, multiple heliostat scans are taken (usually five) from which 15 data points correlating irradiance and brightness are obtained. The increase in data improves the curve fit.

Heliostat initial alignment has some relatively large errors (centroid error up to 1 to 3 meters) and thus some beams barely cover even one radiometer. In this case, power measurement results are not accurate, but the beam centroid data are in general accurate and a bias update can be achieved. Subsequent tests of this redirected beam give more accurate beam power and centroid results.

Shading Corrections. Response over the vidicon tube face normally exhibits a relatively flat maximum near the center and drops off in the outer region. This nonuniformity is corrected by an algorithm that increases the brightness (or DIR number) in the proper proportion, depending on the pixel position. The correction data are obtained by periodically pointing the camera into an integrating sphere that has uniform illumination. An image grab is taken and stored as a corrective "white file." Similarly, an image grab is taken without any light to obtain a black file.

The correction is then applied as a proportional increase of the actual image file, pixel by pixel, based on the response to uniform illumination.

Brightness/Irradiance Correlation. Accurate results are dependent on the correlation of a brightness value obtained at a point on the target with the corresponding irradiance measured at that point at nearly the same instant. Either of two methods is used to accomplish this. The first method uses a shutter at each radiometer, coated with the target paint. When the shutter is open, the radiometer measures the irradiance and immediately after the shutter is closed, the video digitizer takes a "frame grab." The brightness of that particular spot on the beam can then be correlated with the irradiance reading immediately prior to shutter closure. The time between the two measurements is approximately 0.5 to 1 second. This technique is workable for beams having reasonably uniform irradiance and little rapid beam movement. For beams having an irregular irradiance distribution, and beam movement, the correlations show increased scatter. The second method is to leave the shutters open and obtain data on brightness from the adjacent pixels. This approach was originally used for the NWC tests [1]. The average brightness is then correlated with the radiometer reading taken at the same instant. This technique has proven to be more accurate and efforts are planned to improve this technique by reconfiguring the shutter opening and further reducing the time delay.

In principle, the radiometer as seen by the camera is darker than the immediate surrounding target area, but since the radiometer and target hole size can be less than the characteristic dimensions of a pixel (~ 5 cm/pixel), the camera response to this dark region is slight. In addition, iteration techniques are used to determine the brightness that would have been observed at the radiometer, if the target hole were negligibly small and the target reflectance were thus uniform.

Background. The target background irradiance is time and position dependent as a result of incident light variations on the target from the sun, clouds, ground, and especially, wide-angle scattering from the heliostats. The time between a power scan and background scan is approximately 5 to 30 seconds, and slight background changes can occur. Since background area is several times the beam area, a relatively small change in background can introduce a nonnegligible error in net beam power. Several techniques are used to minimize this effect. First, if incident solar irradiance is changing rapidly, a flag is set, alerting an evaluator that conditions may be changing rapidly. Second, the background brightness on the target periphery is monitored continuously and the background values adjusted so as to nearly correspond to the values during the time the individual beam scans were taken. Third, the region outside the beam is examined by an algorithm that adjusts the difference so that it becomes minimal. In effect, the region outside the beam should have a net irradiance of zero when the total irradiance minus the background irradiance is examined.

Sun-Shape Camera Design. The sun-shape camera is located on the control building roof adjacent to an Eppley normal incident pyrheliometer. The sun-shaped camera tracks the sun during BCS data acquisition and measures the solar radiance distribution an instant after the beam data are obtained for each heliostat. All of these data are stored on tape for engineering evaluation purposes, such as comparisons of the

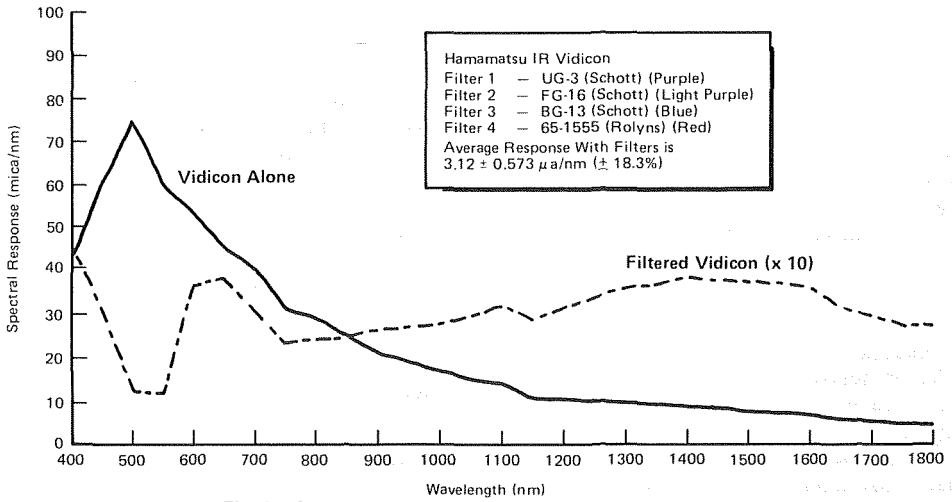

Fig. 3 Corrected camera response with selected filters

Summary of BCS Data 9/13/83												
Helio-stat No.	Centroid average time	Normalized centroid and standard deviation (in.)		Theo power (W)	Power effectivity (%)	Std dev power (%)	Avg spill power (%)	Std dev spill pwr (%)	Invalid data flags	Insol (W/SQM)	Wind speed (mph)	Ambient temp (deg F)
		Horizontal	Vertical									
2903	12:13:41	19.9 ± 9.6	− 9.0 ± 6.2	31125	86.0 ± 1.8	2.1	0.4	0.0	0000000000	886.2	6.8	98.2
2917	12:19:42	33.0 ± 5.4	29.1 ± 1.3	30603	83.4 ± 1.5	1.9	2.0	0.0	0000000000	884.3	7.2	98.5
2904	12:25:24	44.6 ± 4.2	68.5 ± 1.8	31363	72.0 ± 0.9	1.3	11.9	0.0	0000000000	887.0	9.7	99.1
2918	12:31:25	21.1 ± 4.2	−39.1 ± 9.5	31411	89.6 ± 1.2	1.3	1.1	0.0	0000000000	892.4	7.2	99.1
2803	12:37:06	10.0 ± 6.1	−15.0 ± 1.2	31495	87.6 ± 1.1	1.3	2.0	0.0	0000000000	891.1	11.5	99.3
2817	12:42:50	5.7 ± 5.4	−13.7 ± 2.3	31132	84.7 ± 0.9	1.1	0.0	0.0	0000000000	886.9	5.7	99.3
					83.88 ± 6.2							

JOB1 G9015ATABL

Invalid Data Flags Definition	
Position	Definition
1	Horizontal or vertical centroid is greater than 6 ft
2	Standard deviation of the centroid is greater than 2 ft
3	Power effectivity is greater than 100 or less than 60%
4	Percent standard deviation of effectivity is greater than 2.5%
5	Percent standard deviation of measured versus average power is > 2.5%
6	Wind speed is above 20 mph
7	Theoretical power defaulted to 1000.0 watts
8	Default calibration curve used
9	Background update factor not used (default = 1.0)
10	Sunshape data not acquired

JOB1 G9015ATABL

Fig. 4 Typical output summary for operator review

actual and ideal beam irradiance distributions, determination of effects of atmospheric scattering and clouds on solar radiance, and calculations of the solar irradiance that could be redirected to the receiver by an ideal heliostat. These evaluations are critical to the determination of the nature and magnitude of energy losses.

The basic video camera is identical to the BCS field cameras except for the optics, vidicon tube, environmental enclosure, and filters. Camera modifications for elimination of AGC and black-level control are identical and shading corrections are made in the same manner.

A Hamamatsu IR vidicon (N214) is used; it has a spectral response from 400 to 2000 nm and excellent sensitivity in the far red range.

The spectral response characteristics of the Hamamatsu N214 tube show a high peak in the visible and a decrease out to about 2000 nm. However, the sun's radiance has a spectral dependence on radius from the sun's center. Therefore, to obtain a valid radiance distribution for the total sun's radiance over all wavelengths, the tube's spectral response must be corrected by filters to obtain at least a reasonably constant output over its spectral range. A wide variety of off-the-shelf filters was investigated to obtain a set that provided reasonable flatness to the spectral response curve. The filters selected and the response are shown in Fig. 3.

The camera and optics are enclosed in a Lenzar Optics Envirogard housing that uses solid state (Peltier effect) cooling to maintain the enclosure temperature at approximately 10°C (50°F). A Lenzar Optics 200- to 1400-mm zoom lens is used so that a wide range of magnificiations can be obtained.

The camera is mounted on a Meade tracker. Dual-axis corrector controls located at the BCS console allow the operator to position the camera as required for continuous sun tracking. Initial alignment is required each morning of the test day. This simply involves swinging the camera to point at the sun and turning on the tracker. A timer shuts off the tracker late in the afternoon.

The sun-shape camera is calibrated by comparing the sum of the net DIR values to the irradiance over the solid angle corresponding to the Eppley normal incident pyrheliometer (NIP). Thus, knowing the solid angle of each pixel (which is determined by viewing any object of known angle or height and width a given distance from the camera), the calibration coefficients used to transform 8-bit DIR values into absolute radiance units (w/m^2 steradian) is found from

$$K = \frac{I_{\mathrm{NIP}}}{\left\{\sum_{i=10}^{256}\sum_{j=17}^{256}\left[D(i,j)\Big|_{\mathrm{Corrected}} - D(i,j)\Big|_{\mathrm{Black}}\right]\right\}\Delta\theta_x\Delta\theta_y} \tag{1}$$

where

I_{NIP} = Eppley NIP reading (w/m^2).
$D(i,j)\big|_{\mathrm{Corrected}}$ = digital image radiometer intensity (0 to 255 bits) as digitized video signal, corrected for shading
$D(i,j)\big|_{\mathrm{Black}}$ = black level of camera.
$\Delta\theta_x$ = characteristic angle per pixel in the x-direction (horizontal), radians per pixel.
$\Delta\theta_y$ = characteristic angle per pixel in the y-direction (vertical), radians per pixel.

The radiance, $B(i,j)$, in w/m^2 steradian at i, j is thus

$$B(i,j) = \frac{I_{\mathrm{NIP}}\left[D(i,j)\Big|_{\mathrm{Corrected}} - D(i,j)\Big|_{\mathrm{Black}}\right]}{\left\{\sum_{i=10}^{256}\sum_{j=17}^{256}\left[D(i,j)\Big|_{\mathrm{Corrected}} - D(i,j)\Big|_{\mathrm{Black}}\right]\right\}\Delta\theta_x\Delta\theta_y} \tag{2}$$

These results over the entire face of the sun involve as many as 65,000 radiance values. Rather than use these in the computer analysis of the ideal beam shape, a radial distribution is developed and stored on magnetic tape with each heliostat beam scan. Tests of the four radial distributions (right, left, top, and bottom) are conducted to ensure asymmetric sun shape, undistorted by clouds.

Results

Data Display. Since BCS data are required for tracking aimpoint bias updates and for detailed engineering evaluations, the types of data displays vary from data summary sheets to detailed results of beam irradiance distribution over a field of 65,000 pixels, with attendant sun shape data and a complete set of environmental conditions.

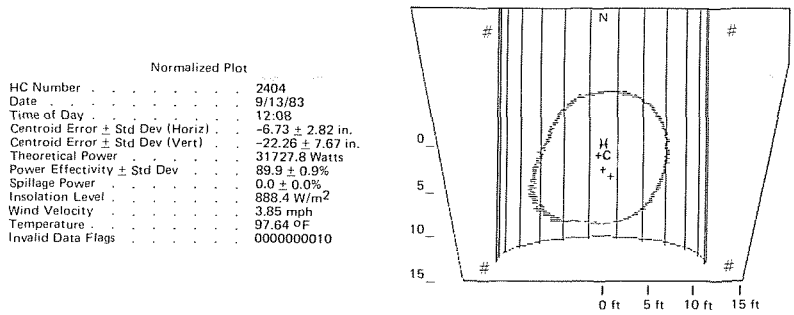

Fig. 5 Typical plot of normalized beam relative to receiver

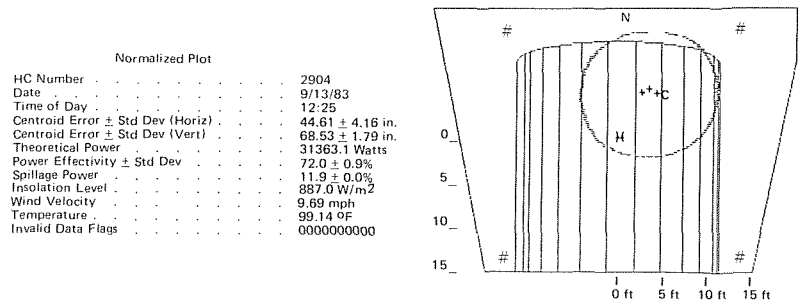

Fig. 6 Typical beam with spillage

The first-level results are given as a summary of BCS data, as shown in Fig. 4. These data are scanned by the operator prior to bias updating. The summary gives the following for each heliostat and time:

1 The beam centroid error as a mean and standard deviation.

2 Theoretical power from that heliostat, at that time, assuming 100 percent reflectance, no atmospheric attenuation, and using the projected area of the tracking heliostat with respect to the plane normal to the ray from the target center to that heliostat.

3 The so-called "power effectivity" which is in principle the same as heliostat reflectance except for additional losses caused by atmospheric attenuation and various scattering losses contributed by soiling, mirror waviness, solar radiance distribution in the circumsolar region, etc.

4 Invalid data flags, if warranted, to caution the operator to examine the results before bias update.

5 Environmental conditions, including wind speed, temperature, and solar insolation as measured by the Eppley normal incident pyrheliometer.

Generally, for bias update purposes, any power effectivity result that is reasonably close to the expected heliostat reflectance (which may vary from 70 to 92 percent depending on degree of mirror cleanliness) is sufficient evidence that the centroid values are valid. Large errors indicate off-nominal occurrences such as no beam on target, multiple beams, etc.

Whether or not bias updating will be applied requires that several additional conditions be met. For example, if the standard deviation of the centroid is large compared with the error and if wind speed is high, it is evident that the heliostat wind-induced oscillations are too large to justify a bias update. Low insolation values, especially values that change significantly from one run to another, imply cloud coverage, and thus bias updates would not be applied until further checks were made.

Trained operators are able to make evaluations rapidly using data such as those shown in Fig. 4. In addition, plots of the beam shape can be generated if additional data are needed to evaluate individual runs. A sample test run is shown in Fig. 5. This run was made shortly after heliostat 2404 was cleaned and its reflectance measured. The BCS value of 89.9 percent

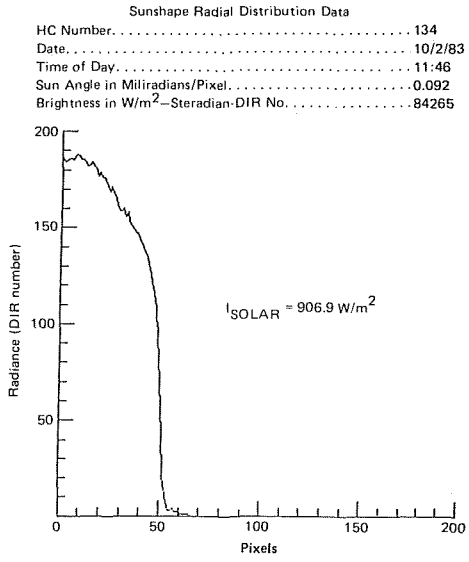

Fig. 7 Typical radial distribution of radiance

compares well with the measured value of 91.8 percent. The beam shape corresponds to the isoflux contour, which contains 90 percent of the net beam power. This is a transformed beam shape (i.e., normalized) as it would appear projected onto a plane normal to the ray from the heliostat to the target. Overlaid on this beam is the view of the cylindrical receiver as seen from the heliostat; that is, in the normal plane. The normalized plot is required since heliostat beams are incident on a given target over the entire quadrant ($\pm 45°$) and these oblique views of the beam do not correspond to the beam distribution on the receiver. Receiver panels are also designated as viewed from the heliostat.

Only the last beam is normally plotted; "C" designates the centroid. The other four centroids are shown as crosses. The aimpoint on the receiver is shown as the symbol "H". This aimpoint is changed by the HAC on the basis of receiver flux distribution requirements. The aimpoint shown corresponds to the aimpoint required at the time the beam is scanned. The trapezoidal figure is the target size and shape as viewed by the

camera. The target outline is not transformed to appear as if viewed from the heliostat.

Figure 6 shows a beam for heliostat 2904 that has large aimpoint errors; consequently, spillage power is significant at 11.9 percent.

A typical sun shape radial radiance distribution curve is shown in Fig. 7. These radial radiance distributions (with the corresponding characteristic angle associated with the pixel) and the calibration coefficient that transforms the DIR numbers (0 to 255) into radiance (w/m^2 steradian) are recorded on magnetic tape. Results are then used in the heliostat analysis codes: HELIOS [4] and CONCEN [8 and 9].

Accuracy. Beam centroid resolution has been demonstrated to be of the order of ± 2 in., or 0.2 milliradians at the nominal heliostat distance of 800 ft. Heliostat beam movement caused by wind and tracking causes variations in centroid for each scan, but for normal operational conditions, the BCS has been found to give accurate beam centroid results whenever test conditions were valid (i.e., the beam tracking on the target, no extraneous beam present, and no significant clouds distorting the beam shape). Generally, the standard devitaion of the centroid is of the order of ± 2 to ± 5 in., for winds of around 10 to 15 mph or less.

Conclusions regarding irradiance measurement accuracy are preliminary. Overall system accuracy is being investigated by comparing results of DIR power effectivity measurements with independent heliostat reflectance measurements. Results to date indicate that power effectivity for clean heliostats under low wind conditions and with smooth flux distributions shows a mean value less than the measured reflectance value by several percent (2 to 4 percent). The standard deviation in power effectivity for the same heliostats measured over a period of several days is of the order of ± 2 to ± 4 percent. Heliostats that are soiled show a lower mean power effectivity (80 to 84 percent) and a standard deviation of ± 5 to ± 6 percent, compared with the reflectance measurements of approximately 85 to 87 percent. However, only a few of the heliostats in the field are monitored for refectance; hence, comparisons of BCS results are made with inferred field average values. Individual heliostats may actually have the occasionally wide reflectance variations (70 to 90 percent) implied by the BCS results. The standard deviation of the five runs taken rapidly in succession is normally less than ± 2 percent. Figure 4 illustrates these observations.

However, the power effectivity accuracy is degraded by wind-induced beam movement and/or heliostat beams having large flux gradients; values of standard deviation of ± 5 to ± 10 percent are usually obtained for these adverse conditions.

Additional Applications

The DIR/BCS can be used for several additional applications. Viewing the receiver should give the approximate incident irradiance, when correlated with receiver-mounted radiometers. This could provide data on nonuniform flux distributions, excessive flux regions, and real-time incident power. The latter results could in principle be used to control receiver flow rates, with the advantage of providing flux distribution data as clouds begin to shadow the field.

Atmospheric attenuation could be monitored by viewing a constant radiance panel located on the target.

The necessity for cleaning heliostats can be determined by monitoring field-averaged power effectivity.

Heliostat response to wind speed and direction can be monitored by correlating centroid-error standard deviations with wind speed. Other engineering data that may be useful include diurnal variations in aimpoint, effects of temperature on mirror module curvature, any observed performance degradations that may occur over long periods of time, and heliostat integrity (i.e., sudden large heliostat tracking errors, changes in beam shape, or power loss).

The sunshape camera could be used with an occulting disk so that the low radiance values in the circumsolar region could be measured, as well as the high radiance values in the solar disk.

Acknowledgment

This work was performed under US Department of Energy Contract Number DE-AC03-798F10499. Technical monitoring was under the direction of D. N. Tanner, J. J. Bartel, and C. L. Mavis of Sandia National Laboratories. M. J. Caraway (MDAC) was responsible for software development.

References

1 Hallet, R. W., and Gervais, R. L., "Central Receiver Solar Thermal Power System," Vol. III, Book 2, SAN-1108-76-8, MDC G6776, McDonnel Douglas Corp., Oct. 1977.

2 Thalhammer, E. D., "Heliostat Beam Characterization System—Update," *ISA/79 Conference Proceedings*, Chicago, IL, Oct. 1979.

3 Phipps, G. S., "Heliostat Beam Characterization System—Calibration Technique," *ISA/79 Conference Proceedings*, Chicago, IL, Oct. 1979.

4 Biggs, F., Vittitoe, C. N., and King, D. L., "Modeling the Beam Characterization System," *ISA/79 Conference Proceedings*, Chicago, IL, Oct. 1979.

5 King, D. L., and Arvizu, D. E., "Heliostat Characterization at the Central Receiver Test Facility," ASME JOURNAL OF SOLAR ENERGY ENGINEERING, Vol. 103, May 1981.

6 King, K. L., "Beam Quality and Tracking Accuracy Evaluation of Second Generation and Barstow Production Heliostats," Sandia Report SAND 82-0181, Aug. 1982.

7 "Pilot Plant Station Manual, 10 MWe Solar Thermal Central Receiver Pilot Plant," RADL Item 2-1, Vol. 1, System Description, SAN/0499-57, MDC G8544, McDonnell Douglas Corp., Dec. 1980, revised Sept. 1982.

8 McFee, R. H., "Power Collection Reduction by Mirror Surface Non-Flatness and Tracking Error for a Central Receiver Solar Power System," *Applied Optics*, Vol. 14, July 1975, p. 1493.

9 McFee, R. H., "Computer Program CONCEN for Calculation of Irradiation of Solar Power Central Receiver," *Proceedings ERDA Solar Workshop on Methods for Optical Analysis of Central Receiver Systems*, Aug. 1977.